

A variable absorption feature in the X-ray spectrum of a magnetar

Andrea Tiengo^{1,2,3}, Paolo Esposito², Sandro Mereghetti², Roberto Turolla^{4,5}, Luciano Nobili⁴, Fabio Gastaldello², Diego Götz⁶, Gian Luca Israel⁷, Nanda Rea⁸, Luigi Stella⁷, Silvia Zane⁵ & Giovanni F. Bignami^{1,2}

¹*Istituto Universitario di Studi Superiori, piazza della Vittoria 15, I-27100 Pavia, Italy.*

²*Istituto di Astrofisica Spaziale e Fisica Cosmica Milano, INAF, via Bassini 15, I-20133 Milano, Italy.*

³*Istituto Nazionale di Fisica Nucleare, Sezione di Pavia, via Bassi 6, I-27100 Pavia, Italy.*

⁴*Dipartimento di Fisica e Astronomia, Università di Padova, via Marzolo 8, I-35131 Padova, Italy.*

⁵*Mullard Space Science Laboratory, University College London, Holmbury St. Mary, Dorking, Surrey RH5 6NT, UK.*

⁶*AIM CEA/Irfu/Service d'Astrophysique, Orme des Merisiers, F-91191 Gif-sur-Yvette, France.*

⁷*Osservatorio Astronomico di Roma, INAF, via Frascati 33, I-00040 Monteporzio Catone, Italy.*

⁸*Institut de Ciències de l'Espai (IEEC-CSIC), Campus UAB, Torre C5, 2a planta, E-08193 Barcelona, Spain.*

Soft- γ -ray repeaters (SGRs) and anomalous X-ray pulsars (AXPs) are slowly rotating, isolated neutron stars that sporadically undergo episodes of long-term flux enhancement (outbursts) generally accompanied by the emission of short bursts of hard X-rays^{1,2}. This behaviour can be understood in the magnetar model³⁻⁵, according to which these sources are mainly powered by their own magnetic energy. This is supported by the fact that the magnetic fields inferred from several observed properties⁶⁻⁸ of AXPs and SGRs are greater than – or at the high end of the range of – those of radio pulsars. In the peculiar case of SGR 0418+5729, a weak dipole magnetic moment is derived from its timing parameters⁹, whereas a strong field has been proposed to reside in the stellar interior^{10,11} and in multipole components on the surface¹². Here we show that the X-ray spectrum of SGR 0418+5729 has an absorption line, the properties of which depend strongly on the star's rotational phase. This line is interpreted as a proton cyclotron feature and its energy implies a magnetic field ranging from 2×10^{14} gauss to more than 10^{15} gauss.

On 2009 June 5 two short bursts of hard X-rays, detected by Fermi and other satellites, revealed the previously unknown source SGR 0418+5729¹³. Subsequent observations with the Rossi X-ray Timing Explorer (RXTE), Swift, Chandra and X-ray Multi-mirror Mission (XMM) Newton satellites found the new SGR to be an X-ray pulsar with a period of ~ 9.1 s and a luminosity of $\sim 1.6 \times 10^{34}$ erg s⁻¹ (in the 0.5–10 keV band and for a distance of 2 kpc)^{13,14}. During the three years after the onset of the outburst, the spectrum softened and the luminosity declined by three orders of magnitude, but remained still too high to be powered by rotational energy^{9,10,14}. The measured spin-down rate of 4×10^{-15} s s⁻¹ translates (under the assumption of rotating magnetic dipole *in vacuo*) into a magnetic field $B = 6 \times 10^{12}$ G at the magnetic equator⁹, a value well in the

range of normal radio pulsars. However, the presence of high-order multipolar field components of 10^{14} G close to the surface has been invoked to interpret the spectrum of the source in the framework of atmosphere models¹². In any case, a strong crustal magnetic field ($> 10^{14}$ G) seems to be required to explain the overall properties of SGR 0418+5729 within the magnetar model^{9,11}.

Hints of the presence of an absorption feature at 2 keV in the spectrum of SGR 0418+5729 were found in the phase-resolved analysis of data (with relatively low-count statistics) from the Swift X-ray Telescope (XRT) taken during 2009 July 12–16¹⁴. Thanks to the large collecting area and good spectral resolution of the European Photon Imaging Camera (EPIC), we were able to perform a more detailed investigation using data collected by XMM-Newton during a 67-ks long observation performed on 2009 August 12, when the source flux was still high (5×10^{-12} erg cm⁻² s⁻¹ in the 2–10 keV band).

To examine the spectral variations as a function of the star’s rotational phase without making assumptions about the X-ray spectral energy distribution of SGR 0418+5729, we produced a phase–energy image by binning the EPIC source counts into energy and rotational phase channels and then normalising to the phase-averaged energy spectrum and pulse profile. The normalised phase–energy image (Fig.1) shows a prominent V-shaped feature in the phase interval ~ 0.1 – 0.3 . This is produced by a lack of counts in a narrow energy range with respect to nearby energy channels, that is, an absorption feature at a phase-dependent energy. The regular shape of the feature in the phase–energy plane as well as its presence in the three independent EPIC detectors (see Supplementary Fig. 5) exclude the possibility that it results from statistical fluctuations in the number of counts or from an instrumental effect. Another absorption feature is visible at low energies at phase ~ 0.5 – 0.6 .

We extracted from the EPIC data the phase-averaged spectrum of SGR 0418+5729, as well as the spectra from 50 phase intervals of width 0.02 rotational cycles, as described in the Supplementary Information. The phase-averaged spectrum can be adequately fit by either a two-blackbody model ($\chi^2_\nu = 1.198$ for 196 degrees of freedom, d.f.) or a blackbody plus power-law model ($\chi^2_\nu = 1.105$ for 196 d.f.), corrected for interstellar absorption (see refs 11 and 12 for other models that can fit the spectrum).

The 15 spectra extracted from the phase intervals 0.1–0.3 and 0.5–0.6, unlike those of the remaining phases, cannot be fitted by a renormalisation of the phase-averaged best-fit model, which gives in most cases null hypothesis probabilities in the range $10^{-4} - 10^{-9}$ (see Supplementary Fig. 4). They are instead well fitted (null hypothesis probability > 0.03) by the addition of a narrow absorption line component, which can be equally well modelled with a Gaussian profile or a cyclotron absorption line model¹⁵ (the improvement obtained by adding a cyclotron component in the phase intervals 0.1–0.3 and 0.5–0.6 can be seen in Supplementary Fig. 4). The best-fit line parameters as a function of phase are shown in Fig. 2 and an example of phase-resolved spectrum is displayed in Fig. 3.

We searched for the phase-dependent absorption feature in all the available X-ray observations of SGR 0418+5729 and found that it was present in the phase interval 0–0.3, and up to higher energies than in XMM-Newton, in RXTE data taken during the first two months of the outburst (see Supplementary Fig. 6).

Absorption features have been observed in the X-ray spectra of various classes of neutron stars^{16–23} and interpreted as being due to either cyclotron absorption (by electrons or protons) or bound–bound atomic transitions. However, variations in the line energy as a function of the rotational phase as large as in SGR 0418+5729 (by a factor ~ 5 in one-tenth of a cycle) have not been seen in any source.

In a neutron star atmosphere, different atomic transitions might be responsible for a phase-variable absorption feature if temperature, elemental abundance or magnetic field vary strongly on the surface. The line energies observed in SGR 0418+5729 (~ 1 – 5 keV) rule out transitions in magnetised H and He, which occur below ~ 1 keV^{24,25}. On the other hand, the absorption spectra of heavier elements are much more complex (see, for example, ref. 26 for C, O and Ne) and some lines could occur at high-enough energies. However, to explain the phase resolved spectra of SGR 0418+5729, the physical conditions of a heavy-element atmosphere are forced to vary in such a way that a single transition should dominate the opacity at each of the phases where the absorption line is detected.

A more straightforward explanation for the line variability can instead be given if the feature is due to cyclotron resonant scattering. The cyclotron energy (in keV) for a particle of charge e and mass m in magnetic field B (in gauss) is given by

$$E_B \approx \frac{11.6}{1+z} \left(\frac{m_e}{m} \right) \left(\frac{B}{10^{12}} \right)$$

where $(1+z)^{-1} = (1 - 2GM_{\text{NS}}/(Rc^2))^{1/2}$ (which is ~ 0.8 at the star surface for typical neutron star mass and radius $M_{\text{NS}} = 1.4 M_{\odot}$ and $R_{\text{NS}} = 12$ km, respectively) accounts for the gravitational redshift at distance R from the neutron star centre, m_e is the mass of the electron, and c is the velocity of light. In this case, the phase variability of the feature energy would simply be due to the different fields experienced by the charged particles interacting with the photons directed towards us as the neutron star rotates.

If the absorbers/scatterers are electrons hovering near the star surface, the expected line energy is ~ 70 keV for the dipole field at the equator of SGR 0418+5729 ($B = 6 \times 10^{12}$ G); this line energy is more than 10 times higher than that observed. A possible way to explain this large discrepancy might be to assume that the electrons producing the line are located higher up in the magnetosphere in a dipolar geometry, where the magnetic field is smaller ($R \approx 3R_{\text{NS}}$ to have $E_B \approx 2$ keV). Moreover, such an electron population should also be nearly mono-energetic, or subrelativistic, in order to prevent Compton scattering from washing out the feature, which would require a mechanism to maintain slowly moving electrons confined in a small volume high in the

magnetosphere.

If the particles responsible for the cyclotron scattering are protons, the energy range of the SGR 0418+5729 spectral feature requires a magnetic field $> 2 \times 10^{14}$ G (it would be even larger for heavier ions). In the framework of the magnetar model, the unprecedented phase-variability of the line energy can be explained by the complex topology of the magnetar magnetospheres, in which global and/or localised twists play an important part⁵. This is particularly true for SGR 0418+5729, which has a weak dipolar component, as testified by the small spin-down value, whereas a much stronger internal magnetic field has been advocated to explain its X-ray luminosity and burst activity^{10,11}. Furthermore, the presence of small-scale, strong, multipolar components of the surface field has been inferred by fitting its phase-averaged X-ray spectrum with models of magnetized neutron star atmospheres¹².

In this context, the observed line variability might be due to the presence of either strong magnetic field gradients along the surface or vertical structures (with a spatially dependent field) emerging from the surface. To work out how the dynamic magnetosphere of a magnetar should look, an analogy with the solar corona in the proximity of sunspots has been proposed (see, for example, ref. 27). In particular, localised, baryon-rich, magnetic structures, in the form of rising flux tubes, or ‘prominences’, produced by magnetic reconnection or the emergence of the internal field near a crustal fault, have been proposed to explain some of the observed properties of the giant flare emitted in 2004 by SGR 1806–20^{28,29}. If a similar scenario, albeit on a reduced scale, occurred during the outburst of SGR 0418+5729, a spectral feature might arise as thermal photons from the hot spot (a small hot region on the neutron star surface, responsible for most of the X-ray emission, which could be itself related to the prominence) cross the plasma threading the magnetic loop. A proton density $\approx 10^{17}$ cm⁻³ is needed to produce a resonant scattering depth of order unity⁵. Protons, being heavy, do not rise much above the surface and move subrelativistically⁵, so resonant scattering in the prominence is likely to produce a narrow feature instead of an extended tail. As the star rotates, photons emitted in different directions pass through portions of the prominence with different magnetic field, density and size, giving rise to the observed variations of the line centroid and width. A simple quantitative model based on this picture is presented in Supplementary Information. Results, obtained with a geometry consistent with the constraints derived from the X-ray pulsed fraction of SGR 0418+5729, are in good agreement with the observed variations of the feature with phase (Fig. 1).

Acknowledgements We thank G. Goggi and C. Paizis for useful discussion. This research is based on data and software provided by the the ESA XMM-Newton Science Archive (XSA) and the NASA/GSFC High Energy Astrophysics Science Archive Research Center (HEASARC). The Authors acknowledge partial funding from INAF through a PRIN 2010 grant and ASI through contract I/032/10/0.

Author Information The authors declare that they have no competing financial interests. Correspondence and requests for materials should be addressed to A.T. (email: andrea.tiengo@iusspavia.it).

1. Mereghetti, S. The strongest cosmic magnets: soft gamma-ray repeaters and anomalous X-ray pulsars. *Astron. Astrophys. Rev.* **15**, 225–287 (2008).
2. Rea, N. & Esposito, P. Magnetar outbursts: an observational review. In Torres, D. F. & Rea, N. (eds.) *High-Energy Emission from Pulsars and their Systems*, Astrophysics and Space Science Proceedings, 247–273 (Springer, Heidelberg, 2011).
3. Thompson, C. & Duncan, R. C. The soft gamma repeaters as very strongly magnetized neutron stars - I. Radiative mechanism for outbursts. *Mon. Not. R. Astron. Soc.* **275**, 255–300 (1995).
4. Thompson, C. & Duncan, R. C. The Soft Gamma Repeaters as Very Strongly Magnetized Neutron Stars. II. Quiescent Neutrino, X-Ray, and Alfvén Wave Emission. *Astrophys. J.* **473**, 322–342 (1996).
5. Thompson, C., Lyutikov, M. & Kulkarni, S. R. Electrodynamics of Magnetars: Implications for the Persistent X-Ray Emission and Spin-down of the Soft Gamma Repeaters and Anomalous X-Ray Pulsars. *Astrophys. J.* **574**, 332–355 (2002).
6. Kouveliotou, C. *et al.* An X-ray pulsar with a superstrong magnetic field in the soft gamma-ray repeater SGR 1806-20. *Nature* **393**, 235–237 (1998).
7. Thompson, C. & Duncan, R. C. The Giant Flare of 1998 August 27 from SGR 1900+14. II. Radiative Mechanism and Physical Constraints on the Source. *Astrophys. J.* **561**, 980–1005 (2001).
8. Vietri, M., Stella, L. & Israel, G. L. SGR 1806-20: Evidence for a Superstrong Magnetic Field from Quasi-Periodic Oscillations. *Astrophys. J.* **661**, 1089–1093 (2007).
9. Rea, N. *et al.* The Outburst Decay of the Low Magnetic Field Magnetar SGR 0418+5729. *Astrophys. J.* **770**, 65 (2013).
10. Rea, N. *et al.* A Low-Magnetic-Field Soft Gamma Repeater. *Science* **330**, 944 (2010).
11. Turolla, R., Zane, S., Pons, J. A., Esposito, P. & Rea, N. Is SGR 0418+5729 Indeed a Waning Magnetar? *Astrophys. J.* **740**, 105 (2011).
12. Güver, T., Göğüş, E. & Özel, F. A magnetar strength surface magnetic field for the slowly spinning down SGR 0418+5729. *Mon. Not. R. Astron. Soc.* **418**, 2773–2778 (2011).
13. van der Horst, A. J. *et al.* Discovery of a New Soft Gamma Repeater: SGR J0418+5729. *Astrophys. J.* **711**, L1–L6 (2010).
14. Esposito, P. *et al.* Early X-ray and optical observations of the soft gamma-ray repeater SGR0418+5729. *Mon. Not. R. Astron. Soc.* **405**, 1787–1795 (2010).
15. Makishima, K. *et al.* Observations of the peculiar hard X-ray transient X 0331+53 (V 0332+53). *Publ. Astron. Soc. Japan* **42**, 295–315 (1990).

16. Truemper, J. *et al.* Evidence for strong cyclotron line emission in the hard X-ray spectrum of Hercules X-1. *Astrophys. J.* **219**, L105–L110 (1978).
17. Heindl, W. A. *et al.* Timing and Spectroscopy of Accreting X-ray Pulsars: the State of Cyclotron Line Studies. In Kaaret, P., Lamb, F. K. & Swank, J. H. (eds.) *X-ray Timing 2003: Rossi and Beyond*, vol. 714 of *American Institute of Physics Conference Series*, 323–330 (AIP Melville, 2004).
18. Turolla, R. Isolated neutron stars: The challenge of simplicity. In Becker, W. (ed.) *Neutron stars and pulsars*, vol. 357 of *Astrophysics and Space Science Proceedings*, 141–163 (Springer Heidelberg, 2009).
19. Haberl, F. *et al.* Evidence for precession of the isolated neutron star RX J0720.4-3125. *Astron. Astrophys.* **451**, L17–L21 (2006).
20. van Kerkwijk, M. H. & Kaplan, D. L. Isolated neutron stars: magnetic fields, distances, and spectra. *Astrophys. Space Sci.* **308**, 191–201 (2007).
21. Bignami, G. F., Caraveo, P. A., De Luca, A. & Mereghetti, S. The magnetic field of an isolated neutron star from X-ray cyclotron absorption lines. *Nature* **423**, 725–727 (2003).
22. Gotthelf, E. V., Halpern, J. P. & Alford, J. The Spin-down of PSR J0821-4300 and PSR J1210-5226: Confirmation of Central Compact Objects as Anti-magnetars. *Astrophys. J.* **765**, 58 (2013).
23. Kargaltsev, O., Durant, M., Misanovic, Z. & Pavlov, G. G. Absorption Features in the X-ray Spectrum of an Ordinary Radio Pulsar. *Science* **337**, 946–949 (2012).
24. Potekhin, A. Y. Hydrogen atom moving across a strong magnetic field: analytical approximations. *Journal of Physics B: Atomic, Molecular and Optical Physics* **31**, 49–63 (1998).
25. Medin, Z., Lai, D. & Potekhin, A. Y. Radiative transitions of the helium atom in highly magnetized neutron star atmospheres. *Mon. Not. R. Astron. Soc.* **383**, 161–172 (2008).
26. Mori, K. & Ho, W. C. G. Modelling mid-Z element atmospheres for strongly magnetized neutron stars. *Mon. Not. R. Astron. Soc.* **377**, 905–919 (2007).
27. Beloborodov, A. M. & Thompson, C. Corona of Magnetars. *Astrophys. J.* **657**, 967–993 (2007).
28. Gelfand, J. D. *et al.* A Rebrightening of the Radio Nebula Associated with the 2004 December 27 Giant Flare from SGR 1806-20. *Astrophys. J.* **634**, L89–L92 (2005).
29. Masada, Y., Nagataki, S., Shibata, K. & Terasawa, T. Solar-Type Magnetic Reconnection Model for Magnetar Giant Flares. *Publ. Astron. Soc. Japan* **62**, 1093–1102 (2010).

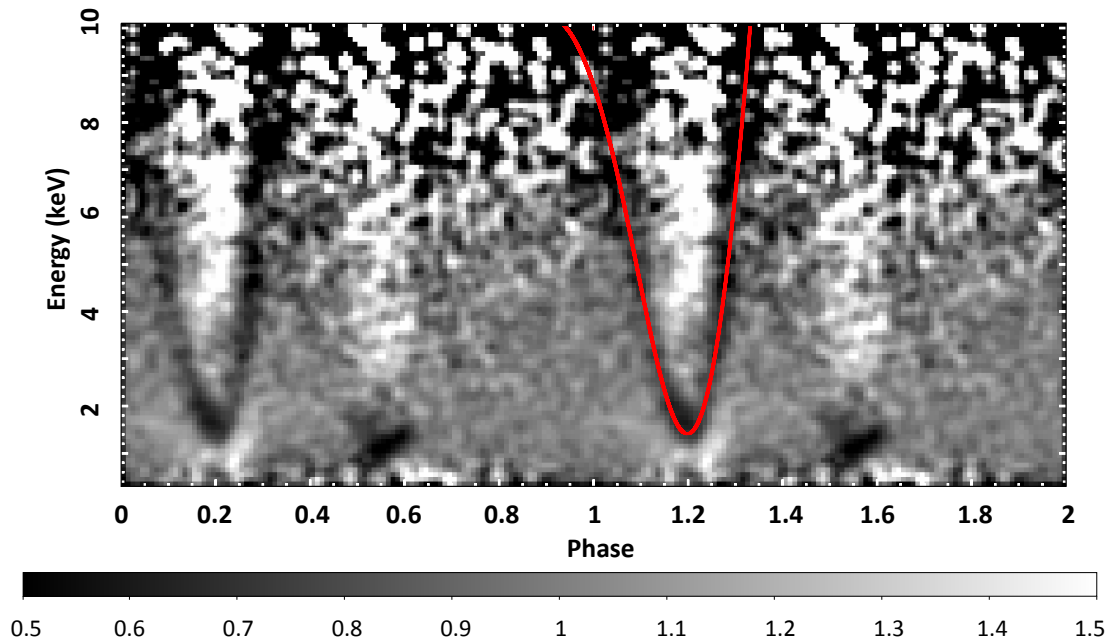


Figure 1: | **Phase-dependent spectral feature in the EPIC data of SGR 0418+5729.** Normalised energy versus phase image obtained by binning the EPIC source counts into 100 phase bins and 100-eV-wide energy channels and dividing these values first by the average number of counts in the same energy bin (corresponding to the phase-averaged energy spectrum) and then by the relative 0.3–10 keV count rate in the same phase interval (corresponding to the pulse profile normalised to the average count rate). The red line shows (for only one of the two displayed cycles) the results of a simple proton cyclotron model consisting of a baryon-loaded plasma loop emerging from the surface of a magnetar and intercepting the X-ray radiation from a small hotspot (see Supplementary Fig. 7 and Supplementary Table 1).

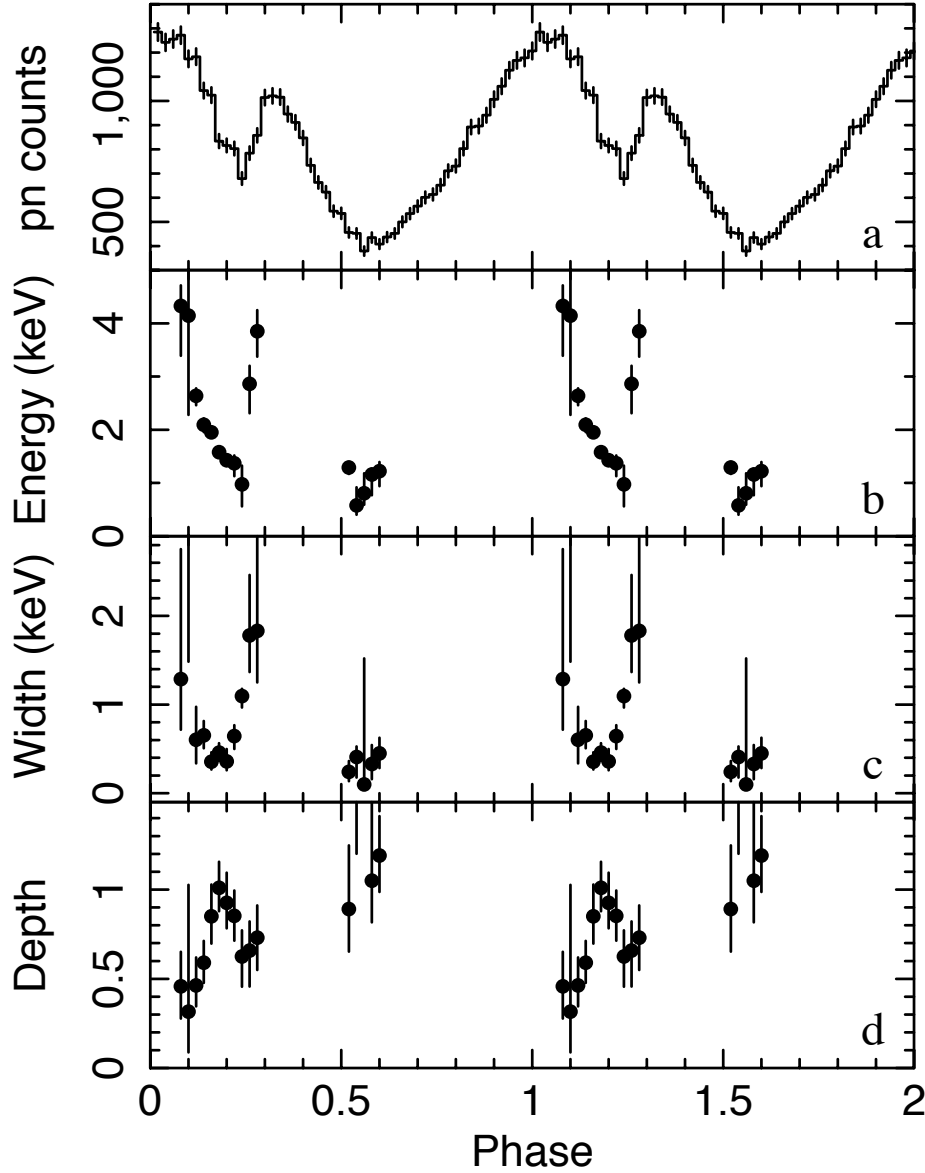


Figure 2: | **Results of the phase-resolved spectroscopy of SGR 0418+5729.** **a**, Pulse profile obtained by folding the 0.3–10 keV EPIC pn light curve at the neutron star spin period $P = 9.07838827$ s. The data points are the number of counts in each phase-dependent spectrum. **b-d**, Line energy (E_c ; **b**), width (W ; **c**) and depth (D ; **d**) of the cyclotron feature as a function of the spin phase. The model consists of a blackbody plus a power law and an absorption line, modified for the interstellar absorption (see Supplementary Information). For the line we used the cyclotron absorption model from ref. 15: $F(E) = \exp\left(-D \frac{(WE/E_c)^2}{(E-E_c)^2 + W^2}\right)$. The interstellar absorption, temperature, photon index and relative normalisations of the two components were fixed to the best-fit values of the phase-integrated spectrum: $N_H = (9.6 \pm 0.5) \times 10^{21} \text{ cm}^{-2}$, $kT = 913 \pm 8$ eV, $\Gamma = 2.8 \pm 0.2$, $(R_{\text{BB}}/d)^2 = 0.81 \pm 0.03 \text{ km}^2 \text{ kpc}^{-2}$ and $K_{\text{PL}} = (1.5 \pm 0.2) \times 10^{-3} \text{ photons cm}^{-2} \text{ s}^{-1} \text{ keV}^{-1}$ at 1 keV. Vertical error bars, 1 s.d.

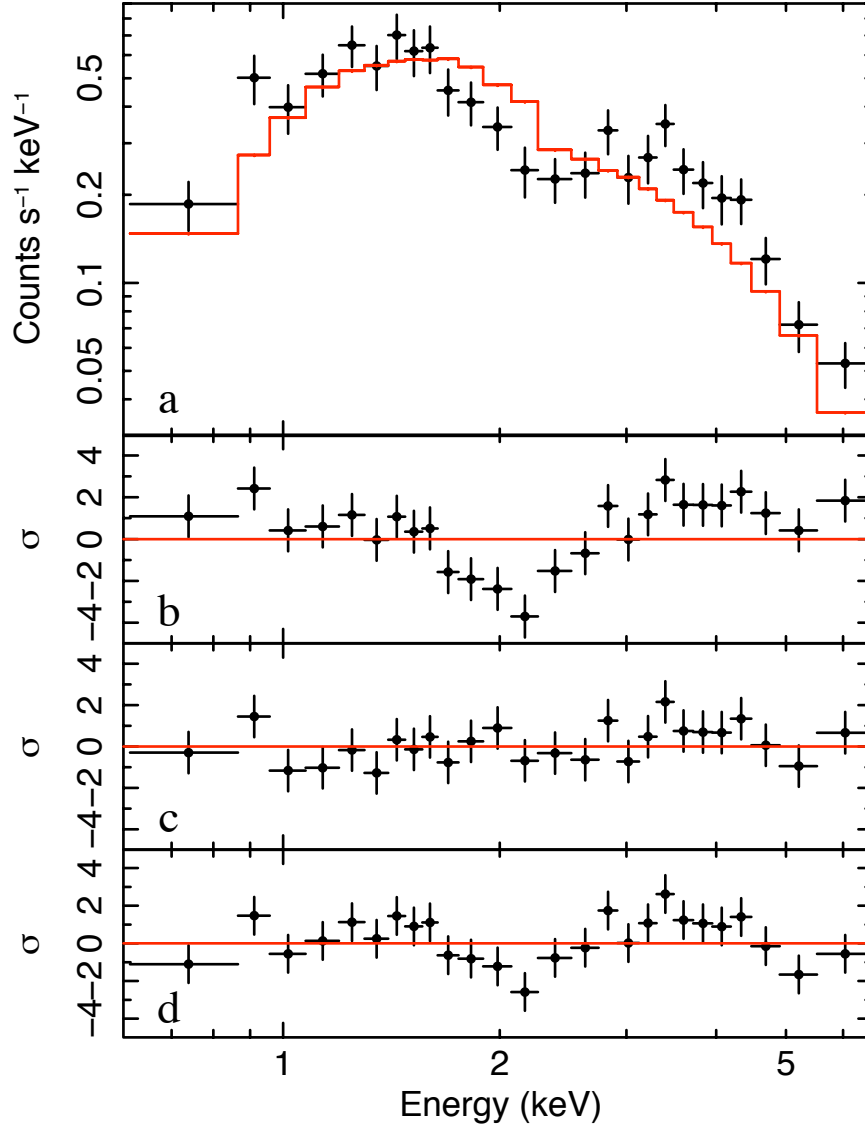


Figure 3: | **Example of a phase-resolved EPIC pn spectrum and its residuals with respect to different models.** **a**, Spectrum from the phase interval 0.15–0.17 (black dots) and best-fit model of the phase-averaged spectrum, rescaled with a free normalisation factor (red line). **b**, Residuals with respect to this model ($\chi^2_\nu = 2.75$ for 25 d.f.); **c**, residuals after the addition of an absorption line (*cyclabs* model in *XSPEC*, with parameters as in Fig. 2; $\chi^2_\nu = 0.94$ for 22 d.f.); **d**, residuals with respect to an absorbed blackbody plus power law model with free temperature, photon index and normalisations ($kT = 1.11 \pm 0.06$ keV and $\Gamma = 3.8 \pm 0.4$; $\chi^2_\nu = 1.75$ for 22 d.f.). This is one of the models (with the same number of free parameters) that we also explored to fit the phased-resolved spectra. In this case, we obtained fits of comparable quality to those with the line model at most phases, but worse fits in the phase interval 0.11–0.21. A joint fit to these five spectra gave an unacceptable χ^2_ν of 1.56 for 116 d.f., to be compared with χ^2_ν of 1.08 for the absorption line model (same number of d.f.). Horizontal error bars indicate the energy channel width; vertical error bars, 1 s.d.; residuals σ are in units of standard deviations.

1 XMM-Newton data analysis

The data have been processed with version 12 of the *Scientific Analysis Software (SAS)* and we used the most recent (2012 October) calibration files available for the EPIC instrument. EPIC consists of two MOS³⁰ and one pn³¹ CCD cameras sensitive to photons with energy between 0.2 and 10 keV. During the 2009 observation (see also Refs. 32, 33), the two MOS and the pn cameras were set in Small Window mode (time resolution of 0.3 s and 5.7 ms, respectively); all detectors were operated with the thin optical blocking filter. Periods in which the particle background was unusually high because of soft proton flares were excluded using an intensity filter. This reduced the net exposure time to 30.7 ks, 50.0 ks and 50.7 ks for pn, MOS1 and MOS2, respectively. Again according to standard procedure, photon event grades higher than 12 for the MOS cameras and 4 for the pn were filtered out. Photon arrival times were converted to the Solar System barycentre reference frame, by using the coordinates³⁴ R.A. = 04^h18^m33.87^s, Decl. = +57°32'22.91" (J2000) and the spin phases were computed with the timing parameters of Ref. 32 ($P = 9.07838827$, Epoch 54993 MJD, valid over the range MJD 54993–55463). The phase–energy images extracted for each of the three EPIC cameras are shown in Fig. 5. The V-shaped feature indicating the presence of a phase-dependent absorption line is present in the three independent datasets.

We also analysed in the same way the three XMM-Newton observations of SGR 0418+5729 performed from September 2010 to August 2012 (the observation settings and the source flux are reported in Ref. 35). However, due to the lower flux, they were not sensitive enough to detect the absorption feature, even if it were still present.

For the source spectra we used the pn counts extracted from a circular region with radius of 35"; the background spectra were extracted from source-free regions on the same chip as the target. The ancillary response files and the spectral redistribution matrices were generated with the *SAS* tasks *arfgen* and *rmfgen*, respectively. For the spectral analysis, performed in the 0.3–10 keV energy range, we used the *XSPEC* fitting package version 12.4³⁶. The abundances adopted were those of Ref. 37 and for the photoelectric absorption we used the cross-sections from Ref. 38.

2 RXTE and Swift data analysis

The RXTE and Swift observations used in this research have been already presented in Ref. 39, to which we refer for more information. All data were reprocessed and analysed with version 6.12 of the *HEAsoft* package and the *CALDB* calibration data base available in 2013 February. Apart from this, the Swift data were reduced exactly as described in Ref. 39.

For each RXTE/PCA data-set, we ran the *xenon2fits* script to combine the GoodXenon files into science event tables with 256 energy bins. We used only data from the Proportional Counter Unit PCU-2, since it is the best-calibrated unit of the PCA instrument, and selected photons from the layer 1 of the detector. We corrected in the event tables the photon arrival times to the Solar System barycentre using the script *fxbary*.

Fig. 6 shows the phase–energy images (rescaled to the phase-averaged spectrum) obtained from PCA observations of SGR 0418+5729 in three different epochs. phase-dependent absorption feature is apparent in the phase interval 0–0.3, and up to higher energies (~ 10 keV) than in XMM-Newton, in the data taken in the first two months after the onset of the outburst, and marginally visible in August 2009 due to the low signal-to-noise ratio. The possible presence of the line at even higher energies cannot be tested due to the very few source photons detected at these energies.

The phase-resolved spectra, with 50 phase bins, were extracted with *fasebin* (which also barycentres the data) and combined with *fbadd*. Consistent phase-averaged spectra were used by the script *pcarsp* to make the 256-bin response matrices, which were combined with *addrmf*. Using the 2009 June–August spectra, we performed a similar analysis as described for the XMM-Newton data. While the results were consistent, owing to the limited spectral capabilities of the PCA instrument the analysis added no new information on the characteristics of the absorption line.

The phase–energy image obtained from the Swift/XRT data taken on 2009 July 12–16 is consistent with the EPIC one. Although the limited spectral capabilities and high instrumental background of the PCA instrument and the poor counting statistics of the XRT data are not adequate for a detailed characterisation of the feature properties, these data indicate that the absorption feature observed with EPIC had been present in the spectrum of SGR 0418+5729 for at least two months.

3 A simple proton cyclotron resonance model

We present here a simple model to illustrate how resonant proton cyclotron scattering can produce a phase-variable absorption feature in the X-ray spectrum of SGR 0418+5729. Let us assume that thermal emission from the star surface comes from a small hot spot (for SGR 0418+5729 the actual angular size is $\sim 4^\circ$ assuming a distance of 2 kpc and a star radius $R_{\text{NS}} = 10$ km; see e.g. Ref. 33) and that an ultra-strong, small-scale magnetic field is present above the spot (the large scale field is a dipole with surface strength $\sim 6 \times 10^{12}$ G). The field is taken to thread a plasma-loaded magnetic loop of radius $r < R_{\text{NS}}$, containing (non-relativistic) protons of density n . For the sake of simplicity, we neglect the loop extent in the radial direction, while retaining a finite transverse width, and assume that the B-field lines are along the loop. Although many different geometries

may be envisaged, in the following the loop is assumed to have the shape of a spherical lune (the round surface of a spherical wedge) with the diameter on the star surface and the spot at its centre, dihedral angle 2β and inclination β_c with respect to the surface normal (see Fig. 7).

Photons of frequency ω emitted by the spot may undergo resonant cyclotron scattering as they traverse the loop and the optical depth is

$$\tau_\omega = \int n\sigma ds = \int n\sigma_T(1 + \cos^2 \theta_{\text{bk}})\delta(\omega - \omega_B) dR, \quad (1)$$

where the expression for the resonant cross section (e.g. Ref. 40) was used, θ_{bk} is the angle between the photon direction and \mathbf{B} , R is the radial coordinate counted from the spot and $\omega_B = eB/(mc)$ is the particle cyclotron frequency. If B is above 10^{12} G, photons in the ~ 1 – 10 keV range can only resonantly scatter on protons. Since we are assuming that matter is confined in a very thin layer at $R = r$ and $\cos \theta_{\text{bk}} = 0$, equation (1) reduces to

$$\tau \sim \frac{\pi^2 enr}{B} \sim 0.4 \left(\frac{n}{10^{17} \text{ cm}^{-3}} \right) \left(\frac{r}{10^5 \text{ cm}} \right) \left(\frac{B}{10^{14} \text{ G}} \right)^{-1}, \quad (2)$$

so a proton density $n \approx 10^{17} \text{ cm}^{-3}$ is required to make the loop thick to resonant scattering. If this occurs, the flux F_ω emitted by the spot will be reduced by a factor $\exp(-\tau_\omega)$ in traversing the baryon-loaded loop. Because only photons with $\omega = \omega_B(r)$ do scatter, this will produce a monochromatic absorption line at $\omega_B(r)$. This is clearly an effect of our approximations. The finite radial extent of both the loop and the emitting spot will result in a broadening of the absorption feature.

Thermal photons are emitted from the spot with a given angular pattern, but only those propagating along the unit vector \mathbf{k} reach the observer; \mathbf{k} is characterized by the angle α it makes with the surface normal and by the associated azimuth ϕ . Because of general relativistic ray bending, α differs from θ , the angle between the line-of-sight (LOS) and the spot normal. We relate them using Beloborodov's approximation⁴¹ (see also Ref. 42)

$$\cos \alpha = \frac{R_S}{R_{\text{NS}}} + \cos \theta \left(1 - \frac{R_S}{R_{\text{NS}}} \right), \quad (3)$$

where R_S is the star Schwarzschild radius.

When the star rotates, both α and ϕ change with the rotational phase $\gamma = 2\pi t/P$, where P is the star spin period. By introducing the angles χ and ξ that the LOS and the spot normal form with the rotation axis, respectively, it is

$$\cos \theta = \cos \xi \cos \chi - \sin \xi \sin \chi \cos \gamma, \quad (4)$$

and

$$\cos \phi = \mathbf{u} \cdot (\mathbf{n} \times \mathbf{k}) / |\mathbf{n} \times \mathbf{k}| = \frac{\sin \gamma \sin \chi}{\sqrt{1 - \cos^2 \theta}}; \quad (5)$$

the latter follows from geometrical considerations (see again Fig. 7; note that the azimuths associated to α and θ coincide) and the last equality holds for \mathbf{u} oriented along the meridian which passes through the spot and pointing north. The angle ϕ is counted from \mathbf{u} and changes by 2π in a cycle if it is $\xi < \chi$ while it oscillates between a minimum and a maximum value (which depend on ξ and χ) in the opposite case.

Because α and θ change during a cycle, the ray direction \mathbf{k} may or may not intersect the loop, so an absorption feature may be present at certain phases only. What actually happens depends on the loop geometry (here its transverse angular width 2β and inclination β_c) and on the angles χ and ξ . Actually, χ and ξ are not known for SGR 0418+5729, the only constraint coming from the measured pulsed fraction ($\sim 50\%$), which implies that their sum is about 90° .

When the ray directed towards the observer crosses the loop, the intersection will occur at different positions according to the phase, giving rise to features at different energies, proportional to the local magnetic field intensity. To obtain a phase–line energy relation to compare with observations, we need to introduce how the magnetic field depends on position in the loop. For simplicity, we assume that the field varies only along the loop, linearly decreasing its intensity as its transverse width increases:

$$B = B_{\max} - f \sqrt{1 - \sin^2 \alpha \cos^2(\phi - \phi_0)}, \quad (6)$$

where B_{\max} is the magnetic field intensity at the base of the loop (where the transverse width vanishes and the field is strongest), f is a multiplicative factor measuring how fast the field varies along the loop and ϕ_0 is the angle between the lune diameter and the meridian passing through the spot.

Selecting convenient combinations of the parameters, our simple analytical model can well reproduce the variation of the line energy with phase observed in SGR 0418+5729, including its relative phase with respect to the maximum of the pulse profile, which occurs at $\gamma \simeq 0.05$ (see Fig. 2) and in our model corresponds to the phase where $\cos \alpha$ is maximum. The red line in Fig. 1 shows the result obtained for a loop with $\phi_0 = 90^\circ$ (i.e., parallel to the equator), $\xi = 20^\circ$, $\chi = 70^\circ$ (consistent with the 50% pulsed fraction), $\beta = 30^\circ$ and $\beta_c = 35^\circ$ (see Table 1 for a list of all the model parameters). The magnetic field in the portion of the loop swept by the line of sight varies from 2.5×10^{14} G to 5×10^{15} G. Although this simple model cannot explain with a single symmetric loop also the low energy line observed at phase ≈ 0.55 , the latter might originate from a second loop with a smaller angular size located on the other side of the hot spot.

30. Turner, M. J. L. *et al.* The European Photon Imaging Camera on XMM-Newton: The MOS cameras. *Astron. Astrophys.* **365**, L27–L35 (2001).
31. Strüder, L. *et al.* The European Photon Imaging Camera on XMM-Newton: The pn-CCD camera. *Astron. Astrophys.* **365**, L18–L26 (2001).
32. Rea, N. *et al.* A Low-Magnetic-Field Soft Gamma Repeater. *Science* **330**, 944 (2010).
33. Turolla, R., Zane, S., Pons, J. A., Esposito, P. & Rea, N. Is SGR 0418+5729 Indeed a Waning Magnetar? *Astrophys. J.* **740**, 105 (2011).
34. van der Horst, A. J. *et al.* Discovery of a New Soft Gamma Repeater: SGR J0418+5729. *Astrophys. J.* **711**, L1–L6 (2010).
35. Rea, N. *et al.* The Outburst Decay of the Low Magnetic Field Magnetar SGR 0418+5729. *Astrophys. J.* **770**, 65 (2013).
36. Arnaud, K. A. XSPEC: The First Ten Years. In Jacoby, G. H. & Barnes, J. (eds.) *Astronomical Data Analysis Software and Systems V*, vol. 101 of *Astronomical Society of the Pacific Conference Series*, 17–20 (ASP, San Francisco, 1996).
37. Wilms, J., Allen, A. & McCray, R. On the Absorption of X-Rays in the Interstellar Medium. *Astrophys. J.* **542**, 914–924 (2000).
38. Balucinska-Church, M. & McCammon, D. Photoelectric absorption cross sections with variable abundances. *Astrophys. J.* **400**, 699 (1992).
39. Esposito, P. *et al.* Early X-ray and optical observations of the soft gamma-ray repeater SGR0418+5729. *Mon. Not. R. Astron. Soc.* **405**, 1787–1795 (2010).
40. Thompson, C., Lyutikov, M. & Kulkarni, S. R. Electrodynamics of Magnetars: Implications for the Persistent X-Ray Emission and Spin-down of the Soft Gamma Repeaters and Anomalous X-Ray Pulsars. *Astrophys. J.* **574**, 332–355 (2002).
41. Beloborodov, A. M. Gravitational Bending of Light Near Compact Objects. *Astrophys. J.* **566**, L85–L88 (2002).
42. Turolla, R. & Nobili, L. Pulse Profiles from Thermally Emitting Neutron Stars. *Astrophys. J.* **768**, 147 (2013).
43. Makishima, K. *et al.* Observations of the peculiar hard X-ray transient X 0331+53 (V 0332+53). *Publ. Astron. Soc. Japan* **42**, 295–315 (1990).

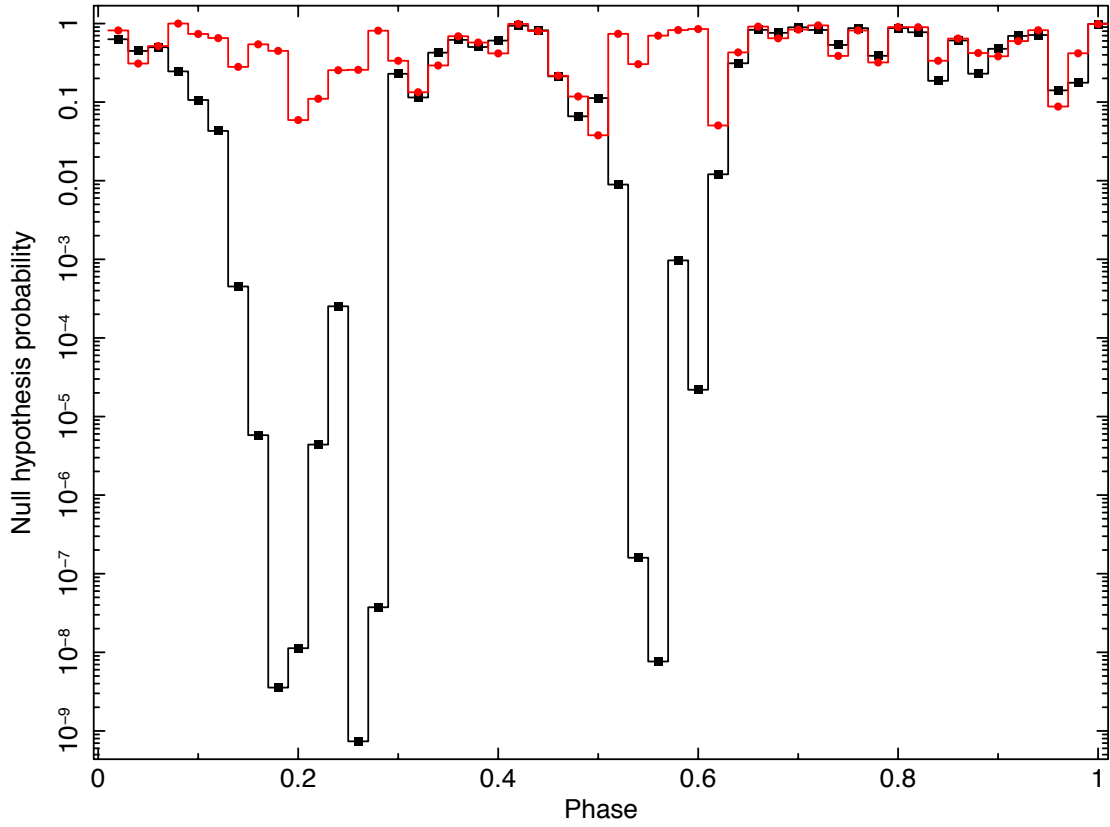


Figure 4: Null hypothesis probabilities derived from the χ^2 and degrees of freedom of the fits of the 50 EPIC pn phase-resolved spectra with two different models: the best-fit model of the phase-averaged spectrum (absorbed blackbody plus power law model, with parameters fixed at the values reported in the caption of Fig. 2) with a free normalisation factor (black) and this same model with the addition of an absorption line (*cyclabs* model⁴³ in *XSPEC*; red).

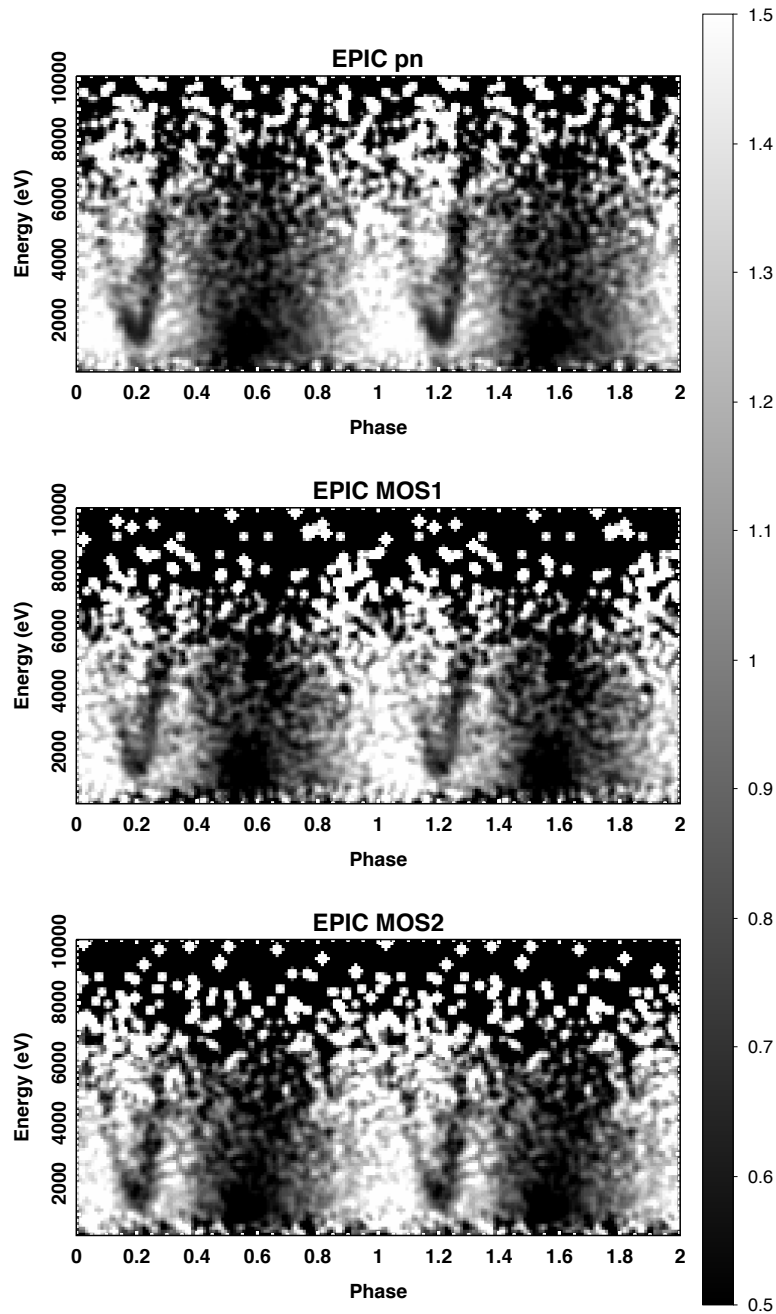


Figure 5: Energy versus phase image obtained by binning the EPIC pn (upper panel), MOS1 (middle panel) and MOS2 (lower panel) source counts into 100 phase bins and energy channels of 100 eV. The number of counts in each phase interval has been divided by the average number of counts in the same energy bin (i.e., the phase-averaged spectrum).

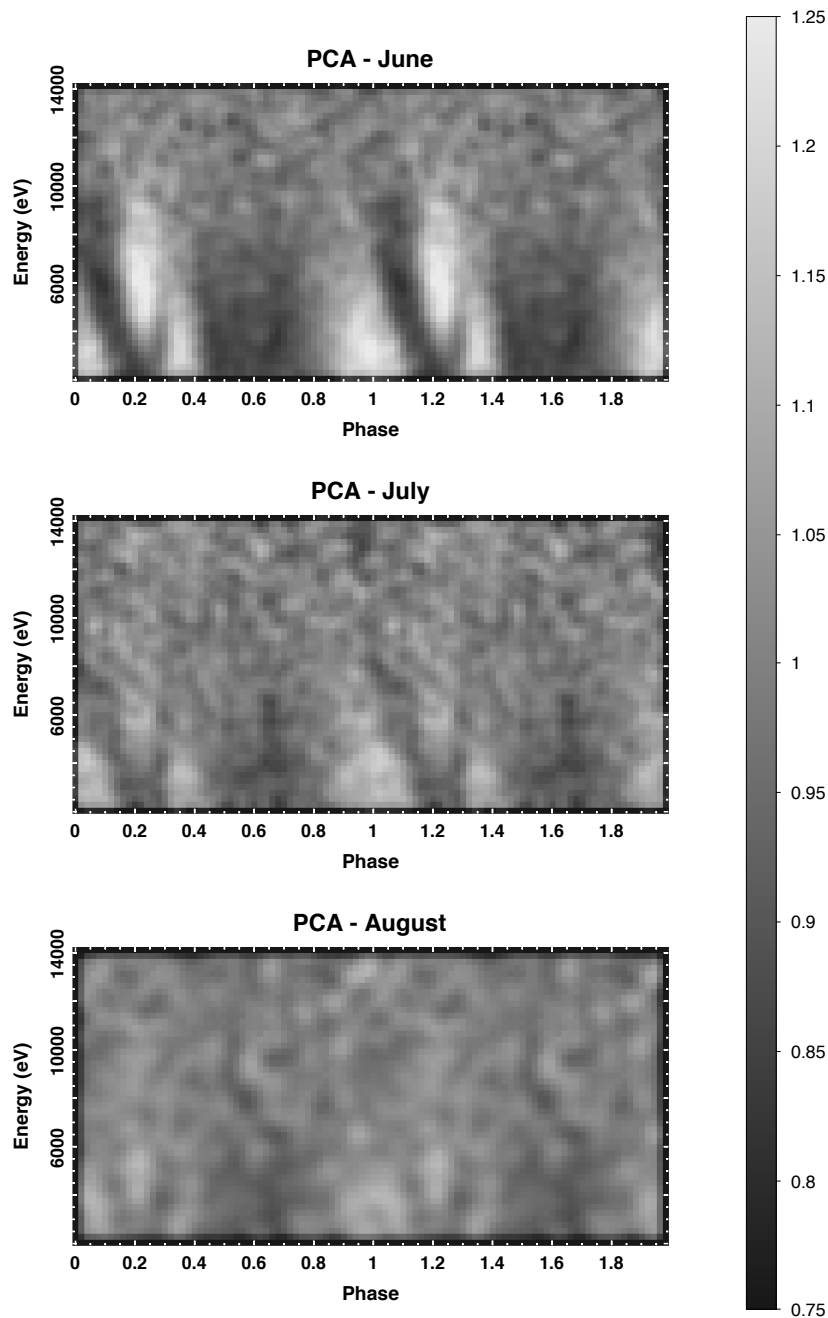


Figure 6: Energy versus phase image obtained by binning the RXTE/PCA data taken in different observations of SGR 0418+5729 (all observations performed in 2009 June, July and August in the upper, middle and lower panel, respectively) into 50 phase bins (two cycles are displayed) and 50 energy channels (channel width 250 eV). The energies within each PCA energy channel have been randomised and the counts in each phase interval divided by the phase-averaged counts in the same energy bin.

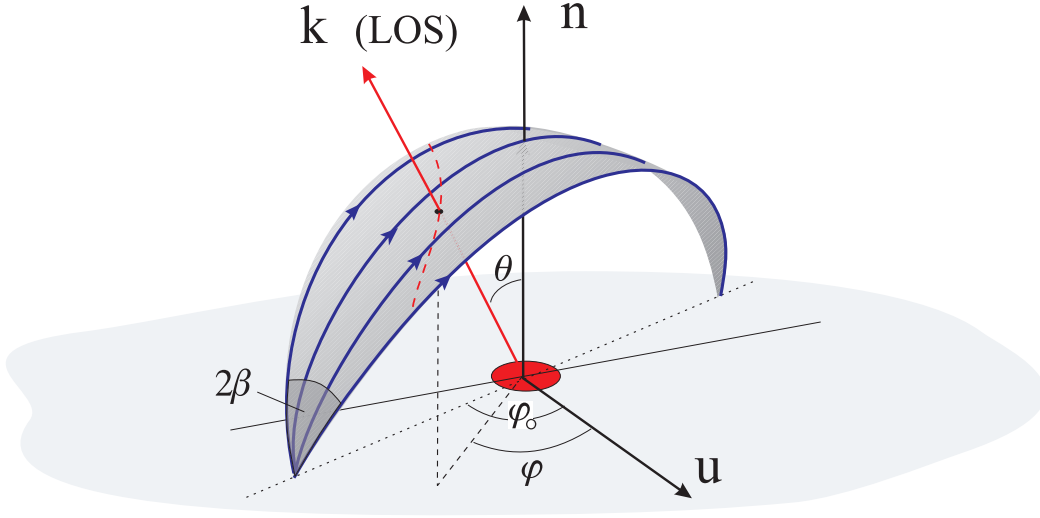


Figure 7: Schematic view of the model discussed in the text. The line-of-sight (LOS) forms an angle θ with the normal to the surface at the spot position, \mathbf{n} , and crosses a magnetic loop oriented at some arbitrary direction with respect to \mathbf{u} . General relativistic ray bending is neglected here, so $\alpha = \theta$. The actual direction of the photon, \mathbf{k}' , differs from \mathbf{k} (see text and equation 3). However, since \mathbf{k}' , \mathbf{k} and \mathbf{n} lie in the same plane, both directions share the same azimuthal angle ϕ .

Table 1: Parameters of the proton cyclotron model producing the line energy variability displayed in Fig. 1 (see Fig. 7 for a schematic view of the model geometry).

Parameter	Description	Value
ξ	Angle between the spot normal and the rotation axis	20°
χ	Angle between the LOS and the rotation axis	70°
ϕ_0	Angle between the lune diameter and the spot meridian	90°
β	Semi-amplitude of the lune transverse angle	30°
β_c	Lune inclination angle	35°
z	Gravitational redshift at the neutron star surface	0.25
B_{\max}	Magnetic field intensity at the base of the loop	7.41×10^{15} G
f	Linear term in Eq. 6	7.16×10^{15} G